Mapping random and systematic errors of satellite-derived snow water equivalent observations in Eurasia

[1]James Foster, [2]Chaojiao Sun, [3]Jeffrey P Walker, [1,2]Richard Kelly, [1,2]Jairui Dong, and [1]Alfred Chang
[1]Hydrological Sciences Branch, Laboratory for Hydrospheric Processes
NASA Goddard Space Flight Center, Greenbelt, Maryland, 20771 USA
[2]Goddard Earth Sciences and Technology Center
University of Maryland Baltimore County, Baltimore, Maryland 21250, USA
[3]Department of Civil and Environmental Engineering
University of Melbourne, Parkville, Victoria, 3010 Australia

ABSTRACT

Passive microwave sensors onboard satellites can provide global snow water equivalent (SWE) observations day or night, even under cloudy conditions. However, there are both systematic (bias) and random errors associated with the passive microwave measurements. While these errors are well known, they have thus far not been adequately quantified. In this study, unbiased SWE maps, random error maps and systematic error maps of Eurasia for the 1990-1991 snow season (November-April) have been examined. Dense vegetation, especially in the taiga region, and large snow crystals (>0.3 mm in radius), found in areas where the temperature/vapor gradients are greatest, (in the taiga and tundra regions) are the major source of systematic error. Assumptions about how snow crystals evolve with the progression of the season also contribute to the errors. In general, while random errors for North America and Eurasia are comparable, systematic errors are not as great for Eurasia as those observed for North America. Understanding remote sensing retrieval errors is important for correct interpretation of observations, and successful assimilation of observations into numerical models.

I.0 INTRODUCTION

Snow plays an important role in the global energy and water budgets, as a result of its high albedo and thermal and water storage properties. Snow is also the largest varying landscape feature of the Earth's surface. Since Eurasia is considerably larger than North America and more of its land mass is positioned in higher latitudes, its snow cover area and snow volume in mid winter are also greater than for North America. Thus, reliable and accurate measurements of snow extent and snow water equivalent (SWE) in Eurasia are essential for climate change studies and for applications such as flood forecasting.

Passive microwave remote sensors onboard satellites provide an all-weather global SWE observation capability day or night. Brightness temperatures from different channels of satellite passive microwave sensors (hereafter referred to as PM) can be used to estimate the snow water equivalent (or snow depth with knowledge of the snow density), and hence snow cover extent. However, there are both systematic (bias) and random errors associated with the passive microwave measurements. In order for the remotely sensed SWE observations to be useful for climate modelers, water resource managers and flood forecasters, it is necessary to have both an unbiased SWE estimate and a quantitative, rather than qualitative, estimate of the uncertainty (Sun et al., 2004). This is a critical requirement for successful assimilation of snow observations into land surface models (LSMs).

For most PM algorithms, the effects of vegetation cover and snow grain size variability are the main source of error in estimating SWE. Forests can have a significant impact on the accuracy of SWE estimates. In densely forested areas, such as the boreal forest of Canada and Siberia, the underestimation of SWE from retrieval algorithms can be as high as 50% (Chang et al., 1996). In addition, snow density and snow crystal size do not remain constant throughout the snow season everywhere on the globe but rather vary considerably over time and space. PM algorithms are found to be very sensitive to snow crystal size (Foster et al., 1999).

The purpose of this paper is to present a methodology for deriving unbiased SWE estimates for Eurasia from PM observations. Both random errors (those that result from simplifying assumptions used in retrieval algorithms) and systematic errors (those due to the effects of vegetation cover and crystal size) are quantified. This paper presents results for the 1990-1991 snow season, as an example, using data from the Special Sensor Microwave/Imager (SSM/I).

2.0 PASSIVE MICROWAVE RADIOMETRY

If a snowpack is not too shallow (> 5 cm or contains more than about 10 mm SWE), scattering of naturally emitted microwave radiation by snow crystals occurs and can be detected at frequencies greater than about 25 GHz. Otherwise, the snow will be virtually transparent. By comparing brightness temperatures detected at an antenna at frequencies greater than 25 GHz (typically scattering dominated) with those brightness temperatures detected at frequencies less than 25 GHz (typically emission dominated), it is possible to identify scattering surfaces. Generally, the strength of scattering signal is proportional to the SWE, and it is this relationship that forms the basis for estimating the water equivalent (or thickness) of a snow pack (Chang et al., 1976; Tsang et al., 2000; Pulliainen and Hallikainen, 2001; Kelly et al., 2003, Foster et al., 2004).

From November 1978 to the present, the SMMR instrument on the Nimbus-7 satellite, and the SSM/I on the Defense Meteorological Satellite Program (DMSP) series of satellites have acquired PM data that can be used to estimate SWE. The SMMR instrument failed in 1987, the year the first SSM/I sensor was placed in orbit. On SMMR, the channels most useful for snow observations are the 18 and 37 GHz channels. For the SSM/I, the frequencies are slightly different (19.35 and 37.0 GHz). The data are projected into ½ degree latitude by ½ degree longitude grid cells, uniformly subdividing a polar stereographic map according to the geographic coordinates of the center of the field of view of the radiometers. Overlapping data in cells from separate orbits are averaged to give a single brightness temperature, assumed to be located at the center of the cell (Armstrong and Brodzik, 1995, Chang and Rango. 2000).

We propose a modified SWE algorithm based on the original algorithm by Chang at al. (1987), where brightness temperature differences between the 19 GHz (or 18 GHz for SMMR) and 37 GHz channels are multiplied by a constant related to the average grain size to derive the water equivalent of the snowpack. The simple algorithm is

$$SWE = c\ (T_{19} - T_{37})\quad [\mathrm{mm}] \tag{1}$$

where SWE is snow water equivalent in mm, c is 4.8 mm K^{-1}, and T_{19} and T_{37} are the horizontally polarized brightness temperatures at 19 GHz (or 18 GHz for SMMR) and 37 GHz, respectively. The performance of this algorithm is similar when either vertical or horizontal polarizations are utilized – horizontal polarization was used in this study (Rango at al., 1979). If the brightness temperature from the 19 GHz channel is less than that from the 37 GHz channel, then the snow depth and SWE are zero (Foster et al., 2004).

To derive snow depth, SWE is simply divided by the snow density. It has been determined that in general, a snow density value of 300 kg/m^3 is representative of mature mid winter snow packs in North America (Foster et al., 1999). The effect of this is to modify the coefficient in (1) such that c is 1.60 cm K^{-1} (1.59 cm K^{-1} for SMMR).

3.0 UPDATED RETRIEVAL ALGORITHM

There are typically two kinds of errors associated with a given observation, systematic error (bias) and random error. In this study, the emphasis is to evaluate the bias in the original algorithm (1) by comparing it with a new algorithm (2). We use the term “bias” as if the new algorithm gives “true” values of SWE – based on evaluations with ground truth data.

The primary source of systematic error in SWE is the masking effect of vegetation, which reduces the brightness temperature difference term in (1). In the PM portion of the electromagnetic spectrum, the error due to forest cover is expected to be very high, upwards of 50%, since the emissivity of the overlying forest canopy can overwhelm the scattering signal from the snowpack (Chang et al., 1996; Brown at al., 2003). Where forests are scant or absent PM estimates of SWE are more accurate.

For each forested pixel, a *fractional forest cover* is calculated using the International Geosphere-Biosphere Program (IGBP) Land Cover Data Set described by Loveland et al. (2000). These data, at 1 km x 1 km, are averaged to the 1° x 1° latitude/longitude grid used in this study. The percentage of forest cover in a PM pixel was calculated from the total number of forest classification pixels at 1 km divided by the total number of pixels. Based on this fractional forest cover, the systematic error in the SWE value obtained from (1) can be estimated. A multiplicative “*forest factor*” is introduced to remove the bias due to forest cover from (1)

$$SWE = F\ c\ (T_{19} - T_{37})\qquad [\mathrm{mm}]. \tag{2}$$

We derived the values of forest factor F by assigning underestimation errors in algorithm (1). In Figure 1, the diamonds denote the underestimation error in (1) due to forest cover. For example, if the fractional forest cover at a given pixel is 65%, we assume (1) underestimates SWE by 30%. These nonlinear values are inexact, but are our best approximations at this time. The error bars are our estimates of uncertainty associated with the underestimation estimate of a particular forest cover fraction. The more mixed the pixel, the more uncertainty there is on the forest influence of the PM signal. In other words, untangling the contribution of the signal due to scattering from the underlying snow and emission from trees is harder to assess when the mixture is more even (Foster et al., 2004).

Figure 2 shows the forest factor F as a function of fractional forest cover fr in Eurasia (maximum of 2.0). Note, we used the same fr for North America (Foster et al., 2004). Note that the F factor increases nonlinearly with forest cover. This is to correct for more severe underestimation of SWE due to dense forest cover. The values for F are based on the underestimation of SWE at different values of fr). For example, for a pixel that is 85% forest covered, the underestimation of SWE by algorithm (1) is assumed to be 50%, which is the amount of SWE underestimation that results when a very dense forest cover is present (Foster et al., 2004).

The secondary source of SWE error results from the retrieval algorithm assumption that snow crystal size and shape is spatially uniform and remains constant throughout the snow season. This assumption is reflected in the original SWE retrieval algorithm (1) that has c is a constant. In fact, the crystal effect varies with location and evolves with time. It should be stated that except when the snowpack is thin, the algorithm overestimates SWE, and thus the errors are positive.

Sturm et al. (1995) have characterized the seasonal snowpack into six classes (tundra, taiga, prairie, maritime, alpine, and ephemeral), based on vegetation and meteorological conditions. In this investigation, we consider the evolution of snow crystal size based on these snow classes. As a result, the c value used in (2) varies with time. For our purposes, it is assumed that crystals grow throughout the snow season – an exception to this is the "ephemeral" snow class. Where temperature and vapor gradients are greater (northern interior climates – taiga, tundra, and prairie snow classes), the rate of growth and the associated crystal size errors are typically larger.

Figure 3 shows the systematic errors for six different "Sturm" snow classes due to grain size variability. For each Sturm snow class calendar month, a percentage error in SWE due to differences in snow crystal size over time is prescribed. While negative values of systematic error denote underestimation of SWE, there is an overestimation, in most cases. This is because the microwave scattering increases as the crystals grow in size throughout the snow season. Therefore, as the snow season progresses, the systematic error in these classes increases. The greatest systematic error occurs in the tundra snow and the least in maritime or ephemeral snow (Foster at al., 2004).

The original constant coefficient c (4.8 mm) is associated with an average crystal size of 0.3 mm (radius). Values of c larger than this indicate that the average crystal size is smaller than 0.3 mm, while smaller values are indicative of larger crystals. The largest uncertainty in c random errors occur in the tundra and prairie during the late winter and early spring period, whereas the smallest uncertainty is for the maritime and ephemeral snow classes.

Notice that for the month of November, the error results in only an underestimation for each snow class. The reason for this is because when the snow cover is shallow (< 5 cm), as it generally is at the beginning of the snow season, microwave radiation at all observed frequencies passes through the snowpack virtually unimpeded.

Figure 4 shows the different values of c for each of the six Sturm snow classes for each month of the snow season from October to May for Eurasia. Note that these values were derived from estimates of snow crystal size-related errors (Figure 3) for North America (Foster et al., 2004).

In summary, to compute unbiased SWE value for each pixel using (2), the forest factor F is first determined based on the forest cover fraction of this pixel, then the c value is assigned based on its snow class category and time of the year. The introduction of forest factor F and time and space-varying c in (2) is to correct the systematic errors in (1) so that only random errors remain.

4.0 RESULTS

Figure 5 is a series of monthly maps for November 1990 through May 1991 showing the monthly average SWE using (2). On these maps, largest SWE values are shown in red and the smallest values in blue. Note that pixels mixing with water (primarily around continental margins) have been designated as snow free, even though they may be snow covered during much of the snow season. Also note that for both the November and December maps, SSM/I data was not available in Nepal and western China (linear north-south swatches). In addition, it should be pointed out that SWE in mountainous areas, such as the Himalayas, is underestimated.

Looking first at November, it can be seen that the snow extends well into central Asia. The tundra and taiga regions are completely snow covered – maritime and prairie regions are partially covered. Typically, in the tundra region and the northern taiga, the snow is deepest at this time of year. SWE values for the most part are less than about 90 mm, but in parts of the Central Siberian Plateau and in the uplands of eastern Siberia, SWE values exceed 120 mm. In the prairie and maritime regions, SWE values are less than about 30 mm.

The December map is similar to the November map except that now snow has expanded further south and west, into the elevated portions of the Middle East and Western Europe. SWE has slightly increased over the Central Siberian Plateau and in parts of western Siberia. Thin snow occasionally covers southwestern Russia and interior areas of China and as well as interior areas of Western Europe (ephemeral snow).

By January, SWE has continued to increase in the taiga and in some maritime and prairie areas, but there has been little increase in tundra regions. Again the deepest snows are found across the Central Siberian Plateau, where maximum SWE values now reach 210 mm. Note the ephemeral nature of the snowpack in Western Europe and southwestern Russia – compare with the December map. In western China, the Tarim Basin (Taklimakan Desert) is also snow free. This arid area is ringed by mountains, which depletes storm systems of their moisture before reaching this basin.

In February, the snow extent covers upwards of ¾ of the continent, and SWE values are generally at their greatest. Most of the taiga of Siberia and northern Scandinavia now exceeds 90 mm. SWE is also observed to increase in the mountainous area between the Black Sea and Caspian Sea (eastern Turkey and northern Iran). By March, the snowpack has begun to recede and by April, only the taiga, alpine and tundra regions have SWE values greater than about 30 mm.

Figure 6 is similar to Figure 5 but in this case, maps of monthly biases (difference between SWE estimate from the new (2) and old algorithm (1) are represented – only maps for November, January, February, and April are shown. Shades of yellow and red indicate that the new algorithm is estimating more SWE than the original algorithm. The pale blue and sage colors show areas where there is little difference in SWE estimates using the two algorithms.

For November, the greatest positive errors (> 60 mm) occur across the Central Siberian Plateau, while slightly smaller positive errors are found throughout the taiga region. In the tundra region, the errors are slightly negative – the original algorithm (1) shows slightly more snow than does the new algorithm (2). This results because smaller crystal sizes (0.3 mm diameter) were prescribed for the tundra, using (1), than is actually the case, and therefore the original algorithm overestimated SWE in this region. There is not much change in December and January compared to the November map, except that the errors are a little smaller in over the Central Siberian Plateau (<60 mm), and in south central Eurasia (steppe or prairie region), the errors are slightly negative. By February, positive errors have increased across over much of the taiga region, particularly in eastern Asia (upwards of 60 mm), and the area of negative errors has also expanded somewhat. The maps for February and March are similar, but by April, there is little difference between (1) and (2). In general, systematic errors are not as great for Eurasia as those observed for North America

Figure 7 shows the random errors for the months of November through April (1990-1991) – only November, January, February, and April are shown. Again, the blue colors are indicative of small errors, and the yellow and reds show areas where the errors are greater. Typically, these errors are greatest where the SWE is highest – in the taiga region and across the Central Siberian Plateau (upwards of 24 mm). Random errors are also greater than about 15 mm in northwestern Russia in November, and errors larger than 9 mm are found from Scandinavia eastward across nearly the entire breadth of Russia. Note that in December, the random errors are actually smaller than in November in the taiga region but larger in Western Europe. By February, the errors have increased across eastern Asia (approaching 21 mm in places), however, they have changed very little over the rest of Eurasia. March is very similar to February, except errors are now larger than about 9 mm in the steppes of southwestern Russia and Kazakhstan. Throughout the winter, in the tundra, maritime and ephemeral regions, the random errors remain small – less than 9 mm. By early spring (April), the errors are smaller than for any month during the fall or winter. Only over the Central Siberian Plateau do the errors exceed 15 mm. It appears that the random errors for North America and Eurasia are comparable in magnitude – usually less than about 24 mm.

5.0 CONCLUSIONS

In this study, unbiased SWE maps, random error maps and systematic error maps of Eurasia for the 1990-1991 snow season (November-April) have been examined. Dense vegetation was shown to be the major source of systematic error, while assumptions about snow crystal size and how crystals evolve with the progression of the season also contribute significant biases. In general, while random errors for North America and Eurasia are comparable, systematic errors are not as great for Eurasia as those observed for North America. As more complete data is available on forest density becomes available separate forest factors could be prescribed for taiga sub-classes to better account for SWE in densely forested areas.

ACKNOWLEDGEMENTS

This work was performed under the auspices of NASA Grant NASA NRA 99-OES-04.

REFERENCES

Armstrong, R. L. and M. J. Brodzik, 1995: An earth-gridded SSM/I data set for cryospheric studies and global change monitoring, Advances in Space Research Vol. 10, 155-163.

Brown, R., B. Brasnett and D. Robinson, Gridded North American monthly snow depth and snow water equivalent for GCM evaluation, Atmos.-Ocean, Vol. 41, 1-14, 2003.

Chang, A. T. C., P. Gloersen, T. Schmugge, T. Wilheit, and J. Zwally, 1976: Microwave emission from snow and glacier ice, Journal of Glaciology, Vol. 16, 23-39.

Chang, A.T.C., J.L. Foster and D.K. Hall, 1987: Nimbus-7 derived global snow cover parameters, Annals of Glaciology, Vol. 9: 39-44.

Chang, A.T.C., J.L. Foster and D.K. Hall, 1996: Effects of forest on the snow parameters derived from microwave measurements during the BOREAS winter field experiment, Hydrological Processes, Vol.10: 1565-1574.

Chang, A.T.C. and Rango, A., 2000: Algorithm Theoretical Basis Document (ATBD) for the AMSR-E Snow Water Equivalent Algorithm, NASA/GSFC, Nov. 2000.

Foster, J. L., D. K. Hall, A. T. C. Chang, A. Rango, W. Wergin, and E Erbe, 1999: Effects of snow crystal shape on the scattering of passive microwave radiation, IEEE Transactions on Remote Sensing, Vol.37 (2), 1165-1168.

Foster, J. C. Sun, J. Walker, R. Kelly, J. Dong, and A. Chang, 2004: Identifying and Mapping Systematic Errors in Passive Microwave Snow Water Equivalent Observations, Proceedings of the International Society of Photogrammetry and Remote Sensing (ISPRS), Istanbul, Turkey, July 2004.

Kelly, R., and A. Chang, L.Tsang, and J. Foster, 2003: A prototype AMSR-E global snow area and snow depth algorithm, IEEE Transactions on Geoscience and Remote Sensing, Vol. 41 (2), 230-242.

Loveland, T. R., B. C. Reed, J. F. Brown, D. O. Ohler, J. Zhu, L. Yang, and J. W. Merchant (2000): Development of a global land cover characteristics dataset, International Journal of Remote Sensing, Vol. 21 (6/7), 1303-1330..

Pulliainen, J. and M. Hallikainen, 2001: Retrieval of regional snow water equivalent from space-borne passive microwave observations, Remote Sensing of Environment, Vol. 75: 76-85.

Rango, A., A. Chang, J. Foster, 1979: The utilization of space-borne radiometers for monitoring snowpack properties, Nordic Hydrology, Vol. 10, 25-40.

Sturm, M., J. Holmgren and G. E. Liston, 1995: A seasonal snow cover classification system for local to regional applications, Journal of Climate, Vol. 8, 1261-1283.

Sun, C., J. Walker and P. Houser, 2004: A methodology for initializing snow in a global climate model: Assimilation of snow water equivalent observations. J. Geophys. Res., 109, D08108, doi:10.1029/2003JD003765.

Tsang, L., C. Chen, A.T.C. Chang, J. Guo and K. Ding, 2000: Dense media radiative transfer theory based on quasicrystalline approximation with applications to passive microwave remote sensing of snow, Radio Science, Vol. 35: 731-749.

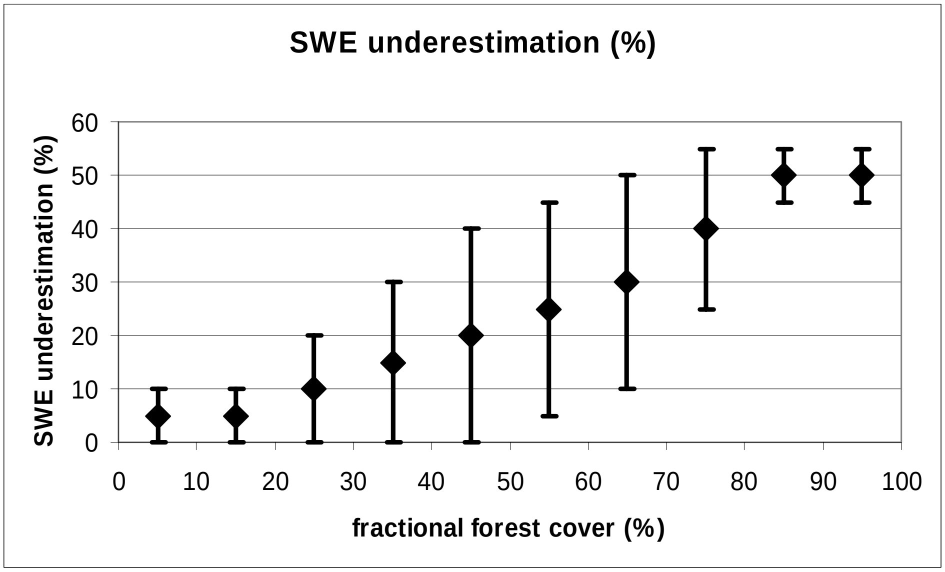

Figure 1. Systematic underestimation and its error bars in unit of percent due to forest cover.

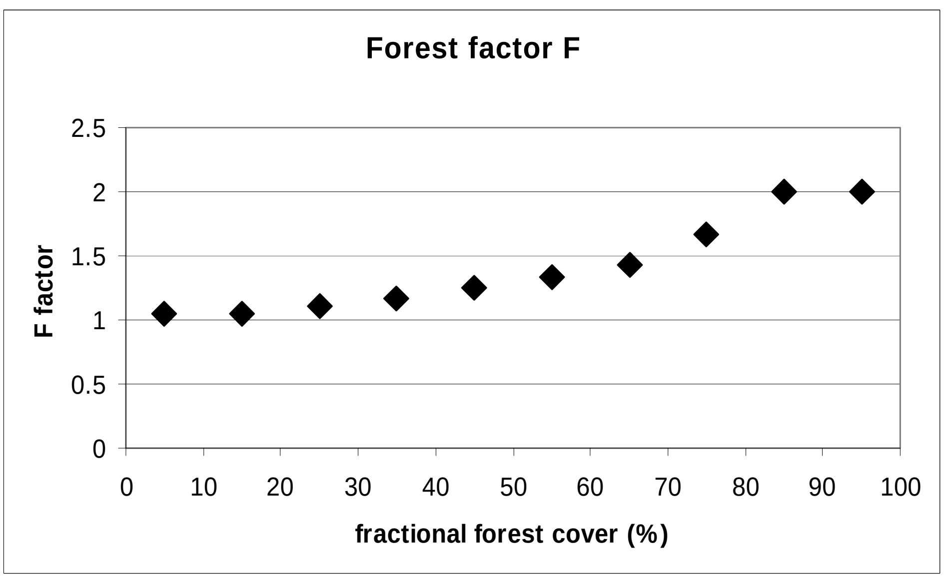

Figure 2. Forest factor *F* as a function of fractional forest cover.

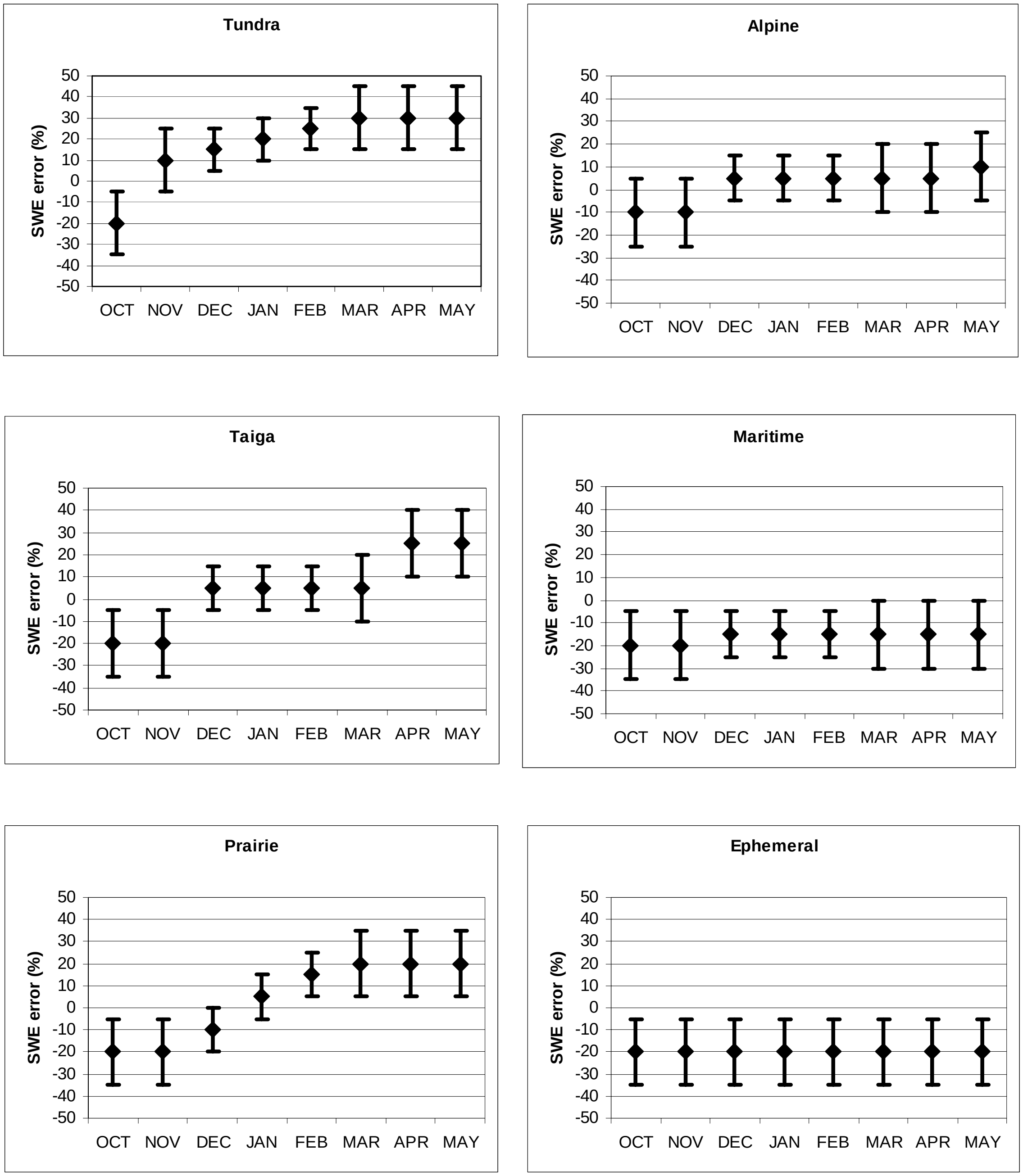

Figure 3. Systematic under-estimation or over-estimation and its error bars in unit of percent due to evolution of snow grain size.

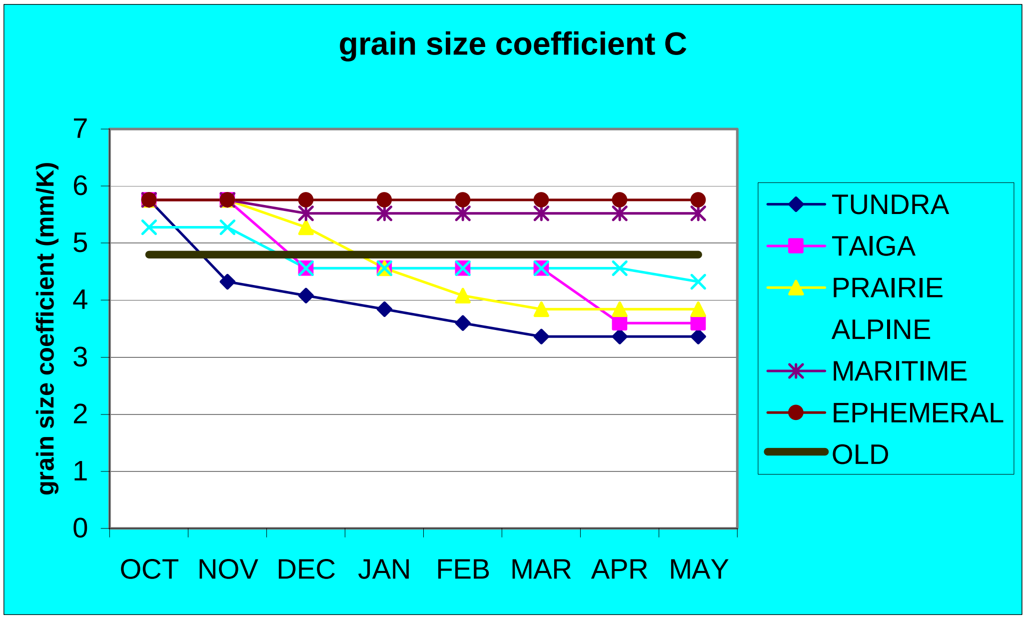

Figure 4. Grain size coefficient c (in mm/K) as a function of month for six Sturm classes. The constant value (4.8 mm/K) used in the original algorithm is also plotted and labeled as "OLD".

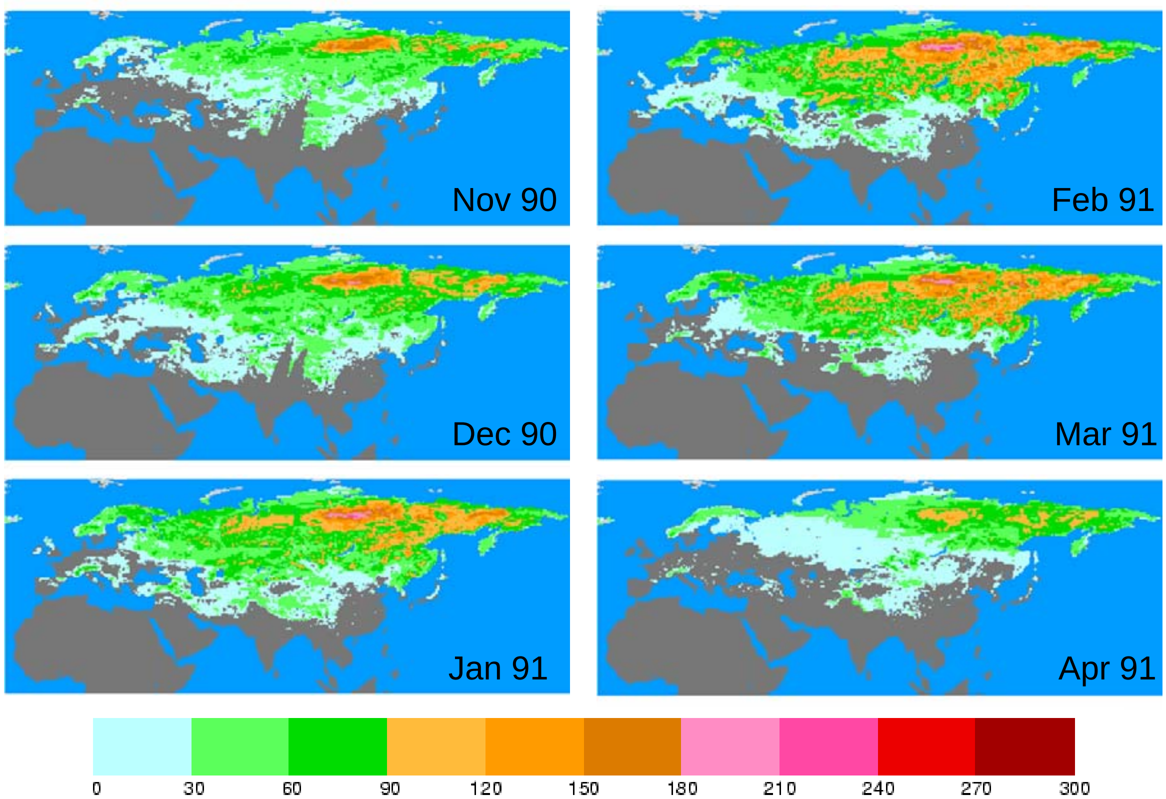

Figure 5: SWE maps from SSM/I during 1990-91 snow season. Snow-free area is dark gray.

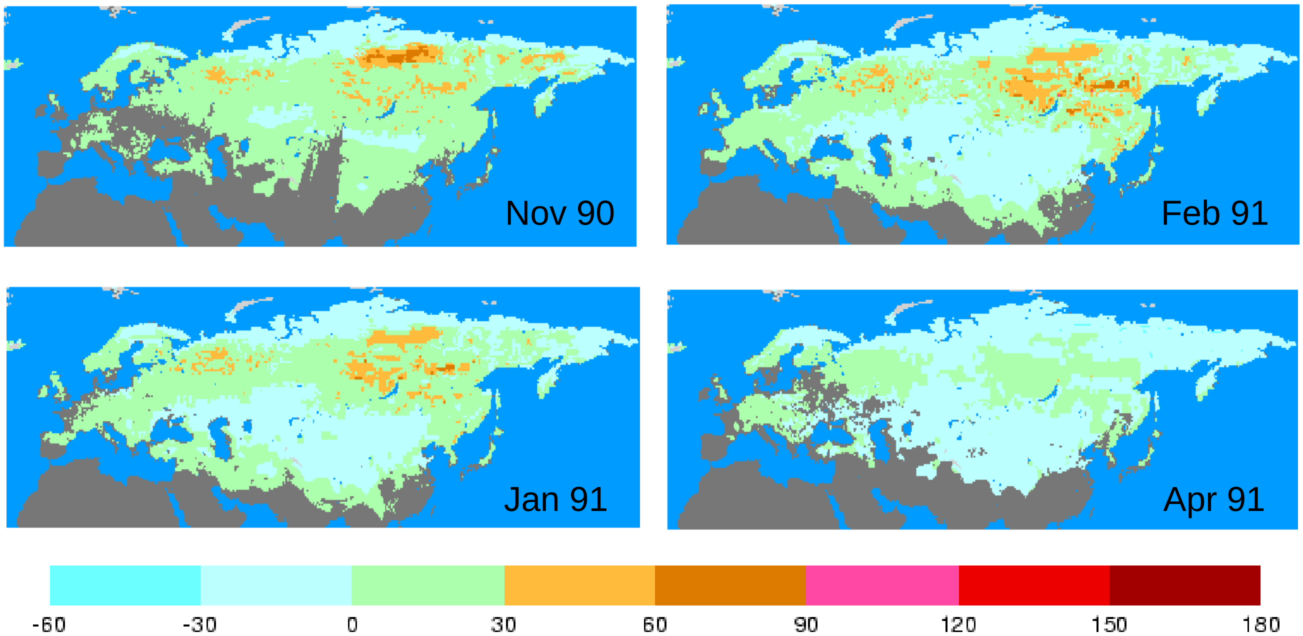

Figure 6: Difference in SWE estimates from two algorithms (new-old) for four selected months during 1990-91 snow season.

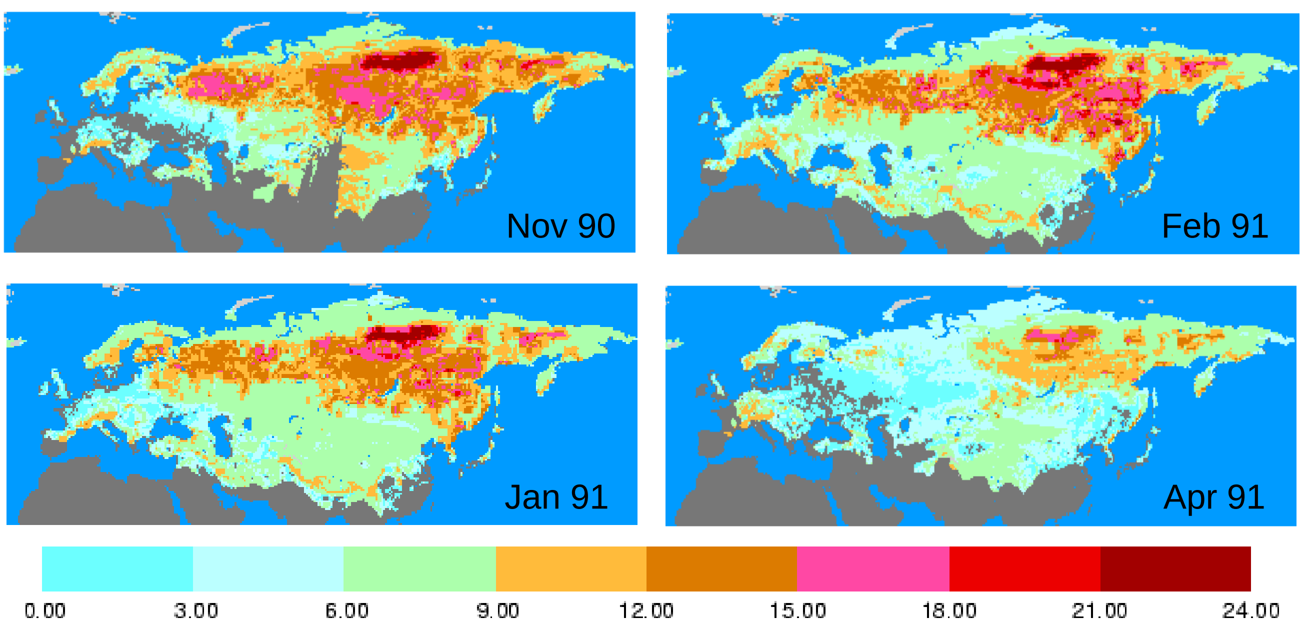

Figure 7: Uncertainty of SWE estimates using the new algorithm for four selected months during 1990-91 snow season.